Dynamical Phase Transitions to Optomechanical Superradiance

Simon B. Jäger,[1] John Cooper,[2,3] Murray J. Holland,[2,3] and Giovanna Morigi[1]
[1]Theoretische Physik, Universität des Saarlandes, D-66123 Saarbrücken, Germany
[2]JILA, National Institute of Standards and Technology and Department of Physics, University of Colorado, Boulder, Colorado 80309-0440, USA
[3]Center for Theory of Quantum Matter, University of Colorado, Boulder, Colorado 80309, USA

(Received 26 November 2018; revised manuscript received 7 May 2019; published 2 August 2019)

We theoretically analyze superradiant emission of light from an ultracold gas of bosonic atoms confined in a bad cavity. A metastable dipolar transition of the atoms couples to the cavity field and is incoherently pumped, and the mechanical effects of cavity-atom interactions tend to order the atoms in the periodic cavity potential. By means of a mean-field model we determine the conditions on the cavity parameters and pump rate that lead to the buildup of a stable macroscopic dipole emitting coherent light. We show that this occurs when the superradiant decay rate and the pump rate exceed threshold values of the order of the photon recoil energy. Above these thresholds superradiant emission is accompanied by the formation of stable matter-wave gratings that diffract the emitted photons. Outside of this regime, instead, the optomechanical coupling can give rise to dephasing or chaos, for which the emitted light is respectively incoherent or chaotic. These behaviors exhibit the features of a dynamical phase transitions and emerge from the interplay between global optomechanical interactions, quantum fluctuations, and noise.

DOI: 10.1103/PhysRevLett.123.053601

Superradiance describes the collective emission of light by an ensemble of dipoles. It is a quantum interference phenomenon in the emission amplitudes [1–3] and is accompanied by a macroscopic coherence within the ensemble [1,2]. In its original formulation, Dicke considered N dipoles confined within their resonance wavelength and showed that their spontaneous decay can be enhanced by the factor N [2].

Quantum interference is typically lost due to fluctuations in the amplitude and in the phase of the dipole-field coupling. These fluctuations can be suppressed by cooling the atomic medium to ultralow temperatures [4,5] and/or by subwavelength localization of the scatterers in an ordered array [6–13]. When, in contrast, the coherence length of the atomic wave function extends over several wavelengths, superradiant scattering of laser light can manifest through the formation of matter-wave gratings [4,5,14–16]. In free space, superradiant gain can be understood as the diffraction of photons from the density grating of the recoiling atoms, which acts as an amplifying medium [4,15]. Within an optical resonator, these dynamics can give rise to lasing [17–20] and be cast in terms of synchronization models [19,21].

In this Letter we analyze the interplay between superradiant emission and quantum fluctuations due to the recoiling atoms, when the atoms' dipolar transitions couple to the mode of a lossy standing-wave resonator. In contrast to Refs. [4,5,14–16], here the atoms are incoherently pumped, as shown in Fig. 1, and therefore no coherence is established by the process pumping energy into the system. The system parameters are in the regime where stationary superradiant emission (SSR) is predicted [22–27]: In a homogeneous medium, SSR consists in the buildup of a stable macroscopic dipole that acts as a stationary source of coherent light. The dynamical properties can be understood in terms of a time-periodic state at

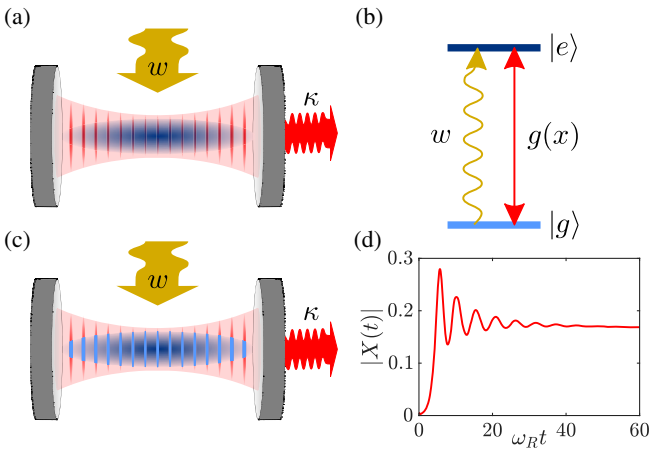

FIG. 1. (a) An atomic gas initially forms a Bose-Einstein condensate and is confined within a standing-wave resonator, which emits photons at rate κ. (b) The metastable atomic transition $|g\rangle \to |e\rangle$ couples to the cavity mode and is incoherently pumped at rate w. After the first superradiant decay (c) the atoms form density gratings. (d) The emitted field $X(t)$ (here in the reference frame of the atomic frequency) becomes coherent for sufficiently large values of w, such that one grating is mechanically stable.

the asymptotics of the driven-incoherent dynamics [28–32], whose frequency is determined by the incoherent pump rate w [28]. In a homogeneous medium the transition from normal to SSR fluorescence is controlled by w when the superradiant decay rate is larger than the rates characterizing other incoherent processes. Here, we show that in the presence of the optomechanical coupling with the external degrees of freedom SSR corresponds to spatiotemporal long-range order and is reached when the characteristic rates exceed the recoil frequency, scaling the mechanical energy exchanged with radiation. When instead the recoil frequency becomes comparable with the pump or the superradiant decay rate, then the superradiant emitted light can become either chaotic or incoherent. The chaotic phase, in particular, characterizes the asymptotic phase of an incoherent dynamics, it emerges from the interplay between quantum fluctuations, noise, and global interactions mediated by the cavity field, and is thus qualitatively different from chaos reported in quantum dynamics of Hamiltonian global-range interacting systems [33,34].

Consider a gas of N atomic bosons with mass m that are confined along the axis of a standing-wave resonator. The atoms do not interact directly; their relevant electronic degrees of freedom (d.o.f.) form a metastable dipole with excited state $|e\rangle$ and ground state $|g\rangle$. The dipoles are incoherently pumped at rate w and strongly coupled to a cavity mode with wave number k and loss rate κ. The evolution of the density matrix $\hat{\varrho}$ for the cavity field and the atoms' internal and external d.o.f. is given by the Born-Markov master equation $\partial_t\hat{\varrho} = [\hat{H}_0 + \hat{H}_c, \hat{\varrho}]/(i\hbar) + w\sum_j \mathcal{L}[\hat{\sigma}_j^\dagger]\hat{\varrho} + \kappa\mathcal{L}[\hat{a}]\hat{\varrho}$. Here, $\hat{H}_0 = \sum_{j=1}^N \hat{p}_j^2/(2m)$ is the total kinetic energy, with $\hat{p}_j$ the momentum of each atom j; $\hat{H}_c = \hbar\Delta\hat{a}^\dagger\hat{a} + \hbar g N(\hat{a}^\dagger\hat{X}/2 + \text{H.c.})$ describes the reversible evolution due to the interaction with the resonator, with $\hat{a}$ and $\hat{a}^\dagger$ the annihilation and creation operators of a cavity photon, and Δ the cavity detuning from the atomic transition frequency. The field couples with strength g to the collective dipole $\hat{X} = \sum_j \hat{\sigma}_j \cos(k\hat{x}_j)/N$, where $\hat{\sigma}_j = |g\rangle_j\langle e|$ and the sum is weighted by the value of the cavity standing-wave mode $\cos(kx)$ at the positions $\hat{x}_j$. The Lindbladians describe the incoherent dynamics and read $\mathcal{L}[\hat{O}]\hat{\varrho} = -(\hat{O}^\dagger\hat{O}\,\hat{\varrho} + \hat{\varrho}\hat{O}^\dagger\hat{O})/2 + \hat{O}\,\hat{\varrho}\,\hat{O}^\dagger$. For $N \gg 1$ the quantum dynamics is numerically intractable due to the adverse Liouville space scaling. This dynamics can be cast in terms of long-range dipolar and optomechanical interactions in the atoms' Hilbert space when κ and Δ are the largest rates. In this regime the atomic transition is radiatively broadened by the coupling with the cavity; its linewidth at an antinode is $\Gamma_c = g^2\kappa/(\kappa^2 + 4\Delta^2)$. Then, the cavity field follows adiabatically the atomic motion, $\hat{a} \propto \hat{X}$ [35,36], while shot-noise fluctuations are negligible [37]. The atoms' density matrix $\hat{\rho}_N$ then obeys the master equation $\partial_t\hat{\rho}_N = [\hat{H}_{\text{eff}}, \hat{\rho}_N]/(i\hbar) + w\sum_j \mathcal{L}[\hat{\sigma}_j^\dagger]\hat{\rho}_N + N\Lambda\mathcal{L}[\hat{X}]\hat{\rho}_N$. Here, $\hat{H}_{\text{eff}} = \hat{H}_0 + \hat{V}$, where $\hat{V} = -\hbar N\Lambda(\Delta/\kappa)\hat{X}^\dagger\hat{X}$ describes the global interactions mediated by cavity photons. Now the incoherent processes are the incoherent pump at rate w and the superradiant decay with rate $\Lambda = N\Gamma_c$. We neglected retardation effects of the cavity field, which is justified by the choice of large κ. We also neglected single-atom radiative decay at rate Γ_c, assuming timescales $t < 1/\Gamma_c$ and $N \gg 1$. Since $1/\Gamma_c = N/\Lambda$, this timescale can be stretched to $t \to \infty$ in a thermodynamic limit $N \to \infty$ where Λ is kept constant [33,36]. Under these assumptions we finally obtain the mean-field master equation for the single-particle density matrix $\hat{\rho}_1$ (assuming that $\hat{\rho}_N$ is a product state at $t = 0$):

$$\partial_t\hat{\rho}_1 = [\hat{H}_{\text{mf}}\{\hat{\rho}_1\}, \hat{\rho}_1]/(i\hbar) + w\mathcal{L}[\hat{\sigma}^\dagger]\hat{\rho}_1, \tag{1}$$

where $\hat{\rho}_1 = \text{Tr}_{N-1}\{\hat{\rho}_N\}$ is obtained by tracing out $N-1$ atoms. Now the incoherent evolution is due entirely to the incoherent pump and the interactions with the resonator are given by the mean-field Hamiltonian:

$$\hat{H}_{\text{mf}} = \frac{\hat{p}^2}{2m} - \frac{\hbar\Lambda}{2\sin\chi}(e^{i\chi}X\{\hat{\rho}_1\}\hat{\sigma}^\dagger + \text{H.c.})\cos(k\hat{x}), \tag{2}$$

with $\tan(\chi) = \kappa/(2\Delta)$. Here, the Rabi frequency is proportional to the mean-field order parameter $X\{\hat{\rho}_1\} = \text{Tr}\{\hat{\sigma}\cos(k\hat{x})\hat{\rho}_1\}$, and thus depends on the global macroscopic dipole. Note that X generates the intracavity field and within the mean-field treatment determines the field's coherence properties. By neglecting the diffusion due to the incoherent pump, Eq. (1) can be reduced to a Vlasov equation with a potential that depends on the macroscopic dipole of the initial state, and whose stable solutions are metastable states of the out-of-equilibrium dynamics [38,39]. In the following we analyze the stability of a thermal initial state $\hat{\rho}_1^{(0)} = |e\rangle\langle e| \otimes \exp(-\beta\hat{p}^2/2m)/Z$, with inverse temperature β, partition function Z. Here, $X\{\hat{\rho}_1^{(0)}\} = 0$.

The short-time dynamics is determined by means of a stability analysis as a function of w and β, see Supplemental Material (SM) [40] for details. No superradiant emission is found when $X\{\hat{\rho}_1^{(0)}\} = 0$ is stable to small fluctuations. When instead $X \sim \exp(\gamma t)$ exponentially increases with $\text{Re}(\gamma) > 0$, then the system undergoes superradiant decay with $\text{Re}(\gamma)$. Figure 2 shows the contour plot of the exponent $\text{Re}(\gamma)$ as a function of both w and β. We find a threshold temperature $k_B T_c \approx 0.1\hbar\Lambda^2/(2\omega_R)$, where $\omega_R = \hbar k^2/(2m)$ is the recoil frequency. For $T > T_c$ thermal fluctuations suppress superradiance. For $T < T_c$ superradiance is found for a finite interval of the pump rate $0 < w \le w_{\max}(\beta)$, which increases with the ratio $\eta = \beta/\bar{\beta} = T_c/T$. For $\eta \to \infty$ the upper bound is $w_{\max} = \Lambda/2$, that coincides with the value found for a homogeneous medium [36]. We now focus on the regime where

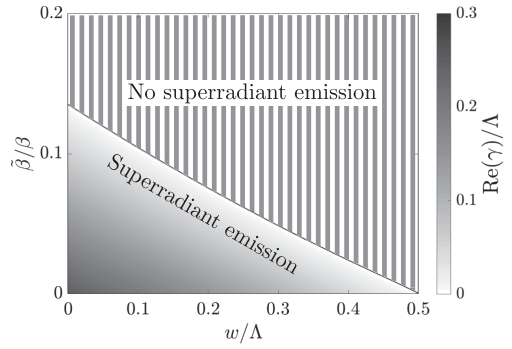

FIG. 2. Contour plot of the rate γ of the first superradiant emission as a function of the incoherent pump rate w (in units of Λ) and of the atomic gas temperature $1/\beta$ [in units of $\tilde{\beta}^{-1} = \hbar\Lambda^2/(2\omega_R)$]. The solid line separates the regime in which the atoms undergo superradiant decay from the one where thermal fluctuations suppress superradiance (stripes).

Λ is of the order of ω_R, so that the threshold temperature T_c can be several μK.

We now study the dynamics of an ensemble of atoms in the zero-temperature limit, when the atoms initially form a Bose-Einstein condensate (BEC). We neglect onsite interactions and analyze the dynamics of the external d.o.f. on the closed family of momentum states $|\Psi_0\rangle = |0\rangle$ (the BEC) and $|\Psi_n\rangle = (|n\hbar k\rangle + |-n\hbar k\rangle)/\sqrt{2}$ $(n = 1, 2, \ldots)$. These states are coupled by absorption and emission of cavity photons; their energy $E_{\mathrm{kin},n} = n^2\hbar\omega_R$ is an integer multiple of ω_R. The asymptotic behavior of Eq. (1) is strictly defined in the thermodynamic limit and is determined by means of a recursive procedure [40]. In Fig. 3 we report the coherence properties of the emitted light in a $w - \Lambda$ phase diagram. We first note the normal (striped) phase with $w > \Lambda/2$, where there is no superradiant emission. The transition from normal to superradiant phase (without optomechanical coupling) has been discussed in the literature [22–24,28,42]. Within the regime where SSR is expected, we now find that the optomechanical coupling gives rise to three phases which we denote by (i) incoherent, (ii) coherent, and (iii) chaotic, corresponding to the coherence properties of the emitted light. In the incoherent phase only the solution with $X = 0$ is stable and collective effects are suppressed. In the coherent phase there is one stable solution with $X \neq 0$. As visible in the phase diagram, the condition for the appearance of this phase is that the superradiant linewidth exceeds a minimum value determined by the recoil frequency, $\Lambda > \Lambda_c$ with $\Lambda_c \sim 6\omega_R$. Finally, the chaotic phase is found for $\Lambda > \Lambda_c$, when the pump rate is below a threshold $w_c(\Lambda)$. Here, both solutions with $X \neq 0$ and $X = 0$ are unstable.

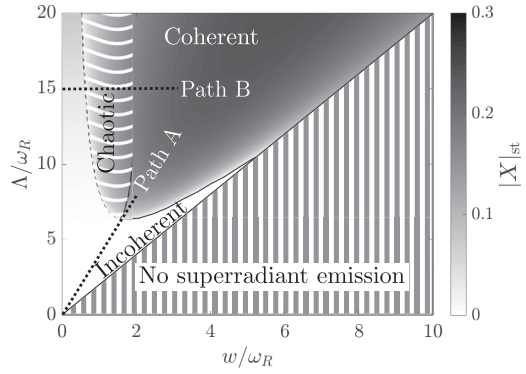

FIG. 3. Phase diagram in the $w/\omega_R - \Lambda/\omega_R$ plane when the atoms initially form a Bose-Einstein condensate at $T = 0$. The phases are labeled by the coherence properties of the emitted light. The emitted field is given by $X(t)$ and is obtained by solving Eq. (1) at the asymptotic dynamics, see [40]. Path A (path B) shows the parameters of Fig. 4 (Fig. 5). In the striped region superradiant decay is suppressed (corresponding to the region at $T = 0$ and $w > \Lambda/2$ in Fig. 2).

We verified these predictions by numerically integrating Eq. (1) with the initial state $\hat{\rho}_1^{(0)}$ at $T = 0$ on the grid of momentum states $p = 0, \pm\hbar k, \ldots, \pm 15\hbar k$. Figure 4(a) displays $|X(t)|$ for different values of Λ along path A of Fig. 3, where a direct transition occurs from an incoherent to a coherent (SSR) phase. For all values the intracavity field $|X(t)|$ first grows exponentially, and subsequently reaches a maximum at a timescale $\tau_c \sim 1/\Lambda$. After this time scale,

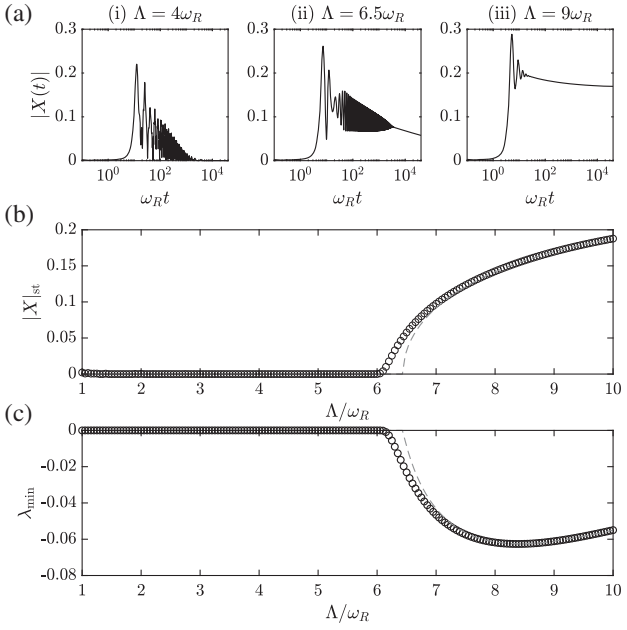

FIG. 4. The incoherent-coherent transition for the parameters of path A of Fig. 3 ($w = \Lambda/4$ and $\Delta = \kappa/2$). Subplot (a), from left to right: Dynamics of X for $\Lambda = 4, 6.5, 9\omega_R$. (b) The asymptotic value for the mean-field order parameter $|X(t_{\mathrm{f}})|$ and (c) the minimum eigenvalue λ_{min} of the partial transpose of the asymptotic density matrix, signalling entanglement between external and internal d.o.f., as a function of Λ (in units of ω_R). Black circles: Numerical results at time $t_{\mathrm{f}} = 4 \times 10^4\omega_R^{-1}$. Dashed lines: Steady-state values from the iterative solution of $\partial_t\hat{\rho}_1 = 0$, Eq. (1).

(i) for $\Lambda < \Lambda_c$ the intracavity field $|X(t)|$ decays to zero. This dynamics is accompanied by the formation of a statistical mixture of states $|e, \Psi_{2n}\rangle$ and $|e, \Psi_{2n+1}\rangle$, which dephases the macroscopic dipole and leads to suppression of superradiant emission. (ii) For $\Lambda \sim \Lambda_c$ the field undergoes fast oscillations and then slowly decays to zero. (iii) For $\Lambda > \Lambda_c$ the field oscillates about a finite asymptotic value and the atoms form a stable spatial pattern. This dynamics exhibits the general features of a dynamical phase transition, which occurs after the first superradiant emission at $t \sim \tau_c$. After τ_c the macroscopic dipole X decays to zero or oscillates about a finite metastable value. We denote the asymptotic value of the order parameter by $X_{\rm st}(\Lambda)$, which we determine by numerical evolution of $|X(t)|$, taking $|X_{\rm st}(\Lambda)| = |X(t_{\rm f})|$, where at $t_{\rm f}$ the dipole $|X(t)|$ has reached a constant value. We compare this result with the asymptotic solution $\hat{\rho}_{\rm st}$ of Eq. (1), using an iterative procedure based on a seed $X > 0$ (as for determining the phase diagram of Fig. 3 [40]). Along path A this iterative procedure always converges to either $X_{\rm st} = 0$ for $\Lambda < \Lambda_c$ and $X_{\rm st} > 0$ for $\Lambda > \Lambda_c$. As is visible in Fig. 4(b), the predictions obtained by numerical integration (circles) and by the iterative procedure (dashed line) qualitatively agree and exhibit the features of a second-order phase transition. Figure 4(c) displays the minimum eigenvalue of the partial transpose of $\hat{\rho}_{\rm st}$. Its behavior shows that at the buildup of SSR internal and external d.o.f. become entangled [40].

The transition separating the coherent from the chaotic phase occurs for $\Lambda > \Lambda_c$ as a function of w: The properties of the emitted light dramatically depend on whether w is smaller or larger than a critical value $w_c(\Lambda)$. Figure 5(a) displays the numerical results for the real and the imaginary part of $X(t)$ for a fixed time interval for (i) $w < w_c$, where the dynamics is chaotic, (ii) $w \simeq w_c$ where the dynamics is mainly characterized by the appearance of two subharmonics, and (iii) for $w > w_c$, where the dynamics is evidently coherent. The spectrum of the emitted light is displayed in Fig. 5(b) as a function of w and for the parameters of path B of Fig. 3. The transition from regular oscillations to chaos occurs at a value w_c where two sidebands appear. We analytically determine w_c by means of a stability analysis; see [40]. This analysis also delivers the frequencies of the sideband at $w = w_c$ and the Lyapunov exponent $\gamma_L = \mathrm{Re}(\gamma)$. As is visible in Fig. 5(c), γ_L changes sign at $w = w_c$ and is positive for $w < w_c$. The trajectory of subplot (a)-(i) corresponds to the value of w where the spectrum is dense: In this parameter regime the stability analysis predicts the transition from chaotic to incoherent dynamics. Numerical simulations show that for $w < w_c$ the density grating becomes unstable and the system jumps back and forth between a prevailing occupation of the set of states corresponding to an even grating, $\{|e, \Psi_{2n}\rangle, |g, \Psi_{2n+1}\rangle, n = 0, 1, 2, \ldots\}$, and of the ones corresponding to an odd grating, $\{|e, \Psi_{2n+1}\rangle, |g, \Psi_{2n}\rangle, n = 0, 1, 2, \ldots\}$. While the states within each set are coupled by coherent processes, the two sets are only coupled to each other by the incoherent pump: Thus, for $w < w_c$ the long-range optomechanical interactions tend to form a grating, which locks the phase of the field, while the incoherent pump induces quantum jumps between different gratings. In the coherent phase internal and external d.o.f. are entangled as soon as $w > w_c$ (see SM also for the analysis of the chaotic phase [40]). We remark that the spin-light dynamics in the coherent phase can be understood in terms of the time crystal studied in Ref. [28]. Our analysis shows that the optomechanical coupling gives rise to a spatial pattern which stabilizes the asymptotic time-periodic state. The parameter regime, however, is smaller than the one predicted in Ref. [28]: the interplay between optomechanical dynamics, noise, and quantum fluctuations gives rise to new time-periodic or even time-aperiodic states.

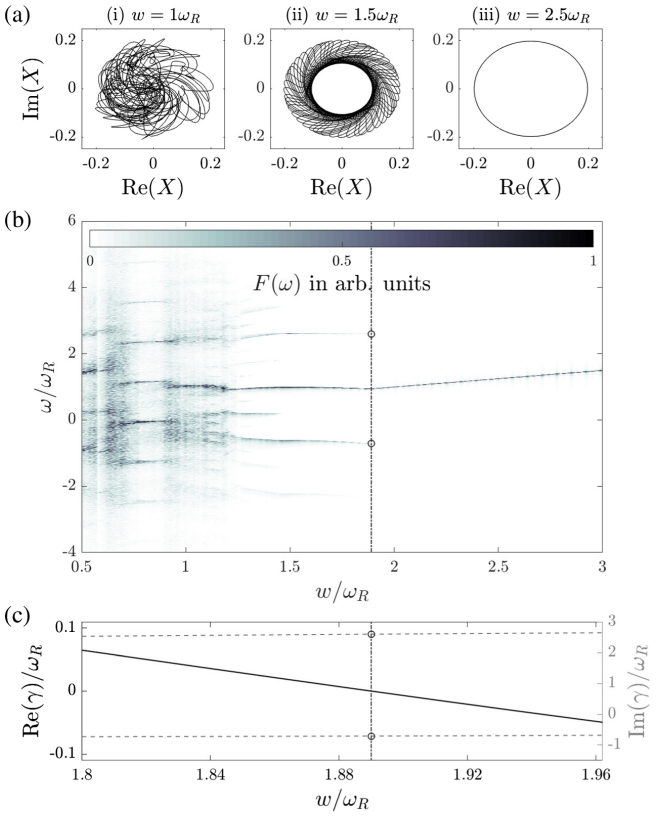

FIG. 5. The chaotic-coherent transition for the parameters of path B of Fig. 3 ($\Lambda = 15\omega_R$ and $\Delta = \kappa/2$). (a) From left to right: real and imaginary parts of X for $w = 1, 1.5, 2.5\omega_R$ (here for the time interval $t \in [9.8 \times 10^3, 10^4]/\omega_R$). (b) Contour plot of the spectrum of the emitted light $F(\omega)$ (arbitrary units) as a function of w and of the frequency ω (in units of ω_R). Here, $F(\omega) \propto |\int_0^{t_{\rm end}} e^{i\omega t} X(t) dt|$ is found by integrating Eq. (1) until $t_{\rm end} = 10^4 \omega_R^{-1}$. (c) The real (solid) and imaginary part (dashed) of the exponent γ (in units of ω_R) giving the stability of the stationary solutions. The vertical dashed lines indicate the critical pumping strength $w_c(\Lambda)$, where $\mathrm{Re}(\gamma)$ changes sign and the sidebands appear; the circles mark the corresponding frequencies.

The phase diagram can be observed by tuning the superradiant linewidth and the pump rate across values of the order of the recoil frequency ω_R; the phases are signaled by the first-order correlation function of the emitted light. These dynamics can be realized when the resonator linewidth κ exceeds by several orders of magnitude ω_R and when other incoherent processes can be discarded over the timescales where the dynamical phase transition occurs. Specifically, the spontaneous decay of the dipolar transition and the particle-particle collision rate shall be orders of magnitude smaller than the recoil frequency, which can be realized using a Raman transition between metastable hyperfine states and low densities, as for instance in Refs. [25,43,44].

The authors are grateful to J. Eschner, L. Giannelli, F. Rosati, S. Schütz, and M. Xu for discussions. This work has been supported by the German Research Foundation (DACH "Quantum crystals of matter and light" and the priority program No. 1929 GiRyd), by the European Commission (ITN "ColOpt") and by the German Ministry of Education and Research (BMBF) via the QuantERA project "NAQUAS." Project NAQUAS has received funding from the QuantERA ERA-NET Cofund in Quantum Technologies implemented within the European Union's Horizon 2020 program. We would like to acknowledge support from the NSF PFC Grants No. PHY 1734006, No. NSF PHY 1806827 and the DARPA Extreme Sensing program.

Note added.—Recently we became aware of Refs. [45–47] where analogous dynamics in similar setups are studied.

[1] M. Gross and S. Haroche, Phys. Rep. **93**, 301 (1982).
[2] R. H. Dicke, Phys. Rev. **93**, 99 (1954).
[3] J. Kim, D. Yang, S.-h. Oh, and K. An, Science **359**, 662 (2018).
[4] S. Inouye, A. P. Chikkatur, D. M. Stamper-Kurn, J. Stenger, D. E. Pritchard, and W. Ketterle, Science **285**, 571 (1999).
[5] K. Baumann, C. Guerlin, F. Brennecke, and T. Esslinger, Nature (London) **464**, 1301 (2010).
[6] W. Vogel and D.-G. Welsch, Phys. Rev. Lett. **54**, 1802 (1985).
[7] R. G. DeVoe and R. G. Brewer, Phys. Rev. Lett. **76**, 2049 (1996).
[8] J. P. Clemens, L. Horvath, B. C. Sanders, and H. J. Carmichael, Phys. Rev. A **68**, 023809 (2003).
[9] S. Fernández-Vidal, S. Zippilli, and G. Morigi, Phys. Rev. A **76**, 053829 (2007).
[10] H. Habibian, S. Zippilli, and G. Morigi, Phys. Rev. A **84**, 033829 (2011).
[11] A. Neuzner, M. Körber, O. Morin, S. Ritter, and G. Rempe, Nat. Photonics **10**, 303 (2016).
[12] S. Begley, M. Vogt, G. K. Gulati, H. Takahashi, and M. Keller, Phys. Rev. Lett. **116**, 223001 (2016).
[13] R. Reimann, W. Alt, T. Kampschulte, T. Macha, L. Ratschbacher, N. Thau, S. Yoon, and D. Meschede, Phys. Rev. Lett. **114**, 023601 (2015).
[14] D. Nagy, G. Kónya, G. Szirmai, and P. Domokos, Phys. Rev. Lett. **104**, 130401 (2010).
[15] D. Schneble, Y. Torii, M. Boyd, E. W. Streed, D. E. Pritchard, and W. Ketterle, Science **300**, 475 (2003).
[16] N. Piovella, R. Bonifacio, B. W. J. McNeil, and G. R. M. Robb, Opt. Commun. **187**, 165 (2001).
[17] R. Bonifacio and L. De Salvo, Nucl. Instrum. Methods Phys. Res., Sect. A **341**, 360 (1994).
[18] R. Bonifacio, L. De Salvo, L. M. Narducci, and E. J. D'Angelo, Phys. Rev. A **50**, 1716 (1994).
[19] S. Slama, S. Bux, G. Krenz, C. Zimmermann, and Ph. W. Courteille, Phys. Rev. Lett. **98**, 053603 (2007).
[20] S. Bux, H. Tomczyk, D. Schmidt, Ph. W. Courteille, N. Piovella, and C. Zimmermann, Phys. Rev. A **87**, 023607 (2013).
[21] C. von Cube, S. Slama, D. Kruse, C. Zimmermann, Ph. W. Courteille, G. R. M. Robb, N. Piovella, and R. Bonifacio, Phys. Rev. Lett. **93**, 083601 (2004).
[22] D. Meiser, J. Ye, D. R. Carlson, and M. J. Holland, Phys. Rev. Lett. **102**, 163601 (2009).
[23] D. Meiser and M. J. Holland, Phys. Rev. A **81**, 033847 (2010).
[24] D. Meiser and M. J. Holland, Phys. Rev. A **81**, 063827 (2010).
[25] J. G. Bohnet, Z. Chen, J. M. Weiner, D. Meiser, M. J. Holland, and J. K. Thompson, Nature (London) **484**, 78 (2012).
[26] D. A. Tieri, M. Xu, D. Meiser, J. Cooper, and M. J. Holland, arXiv:1702.04830.
[27] K. Debnath, Y. Zhang, and K. Mølmer, Phys. Rev. A **98**, 063837 (2018).
[28] K. Tucker, B. Zhu, R. J. Lewis-Swan, J. Marino, F. Jimenez, J. G. Restrepo, and A. M. Rey, New J. Phys. **20**, 123003 (2018).
[29] F. Iemini, A. Russomanno, J. Keeling, M. Schirò, M. Dalmonte, and R. Fazio, Phys. Rev. Lett. **121**, 035301 (2018).
[30] H. Keßler, J. G. Cosme, M. Hemmerling, L. Mathey, and A. Hemmerich, Phys. Rev. A **99**, 053605 (2019).
[31] B. Zhu, J. Marino, N. Y. Yao, M. D. Lukin, and E. A. Demler, arXiv:1904.01026.
[32] Z. Gong, R. Hamazaki, and M. Ueda, Phys. Rev. Lett. **120**, 040404 (2018).
[33] C. Emary and T. Brandes, Phys. Rev. E **67**, 066203 (2003).
[34] A. Lerose, J. Marino, B. Zunkovic, A. Gambassi, and A. Silva, Phys. Rev. Lett. **120**, 130603 (2018).
[35] M. Xu, S. B. Jäger, S. Schütz, J. Cooper, G. Morigi, and M. J. Holland, Phys. Rev. Lett. **116**, 153002 (2016).
[36] S. B. Jäger, M. Xu, S. Schütz, M. J. Holland, and G. Morigi, Phys. Rev. A **95**, 063852 (2017).
[37] H. Habibian, A. Winter, S. Paganelli, H. Rieger, and G. Morigi, Phys. Rev. Lett. **110**, 075304 (2013).
[38] Y. Levin, R. Pakter, F. B. Rizzato, T. N. Teles, and F. P. C. Benetti, Phys. Rep. **535**, 1 (2014).
[39] A. Campa, T. Dauxois, and S. Ruffo, Phys. Rep. **480**, 57 (2009).
[40] See Supplemental Material at http://link.aps.org/supplemental/10.1103/PhysRevLett.123.053601, which includes Refs. [39,41], for further details.
[41] R. Horodecki, P. Horodecki, M. Horodecki, and K. Horodecki, Rev. Mod. Phys. **81**, 865 (2009).

[42] D. Barberena, R. J. Lewis-Swan, J. K. Thompson, and A. M. Rey, Phys. Rev. A **99**, 053411 (2019).
[43] R. M. Kroeze, Y. Guo, V. D. Vaidya, J. Keeling, and B. L. Lev, Phys. Rev. Lett. **121**, 163601 (2018).
[44] M. Landini, N. Dogra, K. Kroeger, L. Hruby, T. Donner, and T. Esslinger, Phys. Rev. Lett. **120**, 223602 (2018).
[45] N. Dogra, M. Landini, K. Kroeger, L. Hruby, T. Donner, and T. Esslinger, arXiv:1901.05974.
[46] E. I. R. Chiacchio and A. Nunnenkamp, Phys. Rev. Lett. **122**, 193605 (2019).
[47] V. Ceban, P. Longo, and M. A. Macovei, Phys. Rev. A **95**, 023806 (2017).